Supporting Information

Plasmon-mediated Catalytic O_2 Dissociation on Ag Nanostructures: Hot Electrons or Near Fields?

Bhogeswararao Seemala[a], Andrew J. Therrien[a], Minhan Lou[b,c], Kun Li[a], , Jordan P. Finzel[a], Ji Qi[a], Peter Nordlander[b-f], Phillip Christopher[a]*

[a]Department of Chemical Engineering, University of California, Santa Barbara, Santa Barbara, California 93117, United States.

[b]Department of Electrical and Computer Engineering, Rice University, Houston, TX 77005, USA.

[c]Laboratory for Nanophotonics, Rice University, Houston, TX 77005, USA.

[d]Department of Chemistry, Rice University, Houston, TX 77005, USA.

[e]Department of Physics and Astronomy, Rice University, Houston, TX 77005, USA.

[f]Department of Materials Science and Nano Engineering, Rice University, Houston, TX 77005, USA

*Email: pchristopher@ucsb.edu

Content

1. Materials, Catalyst synthesis and characterization

1.1 Materials. Silver nitrate (≥ 99.8% purity, Sigma Aldrich, ACS reagent, CAS no. 7761-88-8), sodium citrate tribasic dehydrate (≥ 99.5% purity, Sigma Aldrich, CAS no. 6132-04-3), tannic acid (Sigma Aldrich, ACS reagent, CAS no. 1401-55-4), Ammonium hydroxide solution (Sigma Aldrich, 28.0 – 30.0% NH_3 basis, CAS no. 1336-21-6), Tetraethyl orthosilicate(TEOS) (≥ 99.0% (GC), Aldrich, CAS no. 78-10-4), and ethanol (Fisher Scientific, molecular biology grade) were used for synthesizing the Ag and SiO_2 nanoparticles.

1.2 Synthesis of Ag nanoparticles. Ag nanoparticles (NPs) were synthesized by following the seed-growth method described previously with minor modifications.[1] Ag seeds of 14.1 ± 2.3 nm in diameter were prepared by adding 1 mL of $AgNO_3$ (25 mM) into a boiling aqueous solution (100 mL) containing sodium citrate (5 mM) and tannic acid (0.25 mM) under vigorous stirring. The seed solution was cooled to 80 °C, followed by a sequential injection of sodium citrate, tannic acid, and $AgNO_3$, to further grow the particles. This process was repeated several times for larger Ag NPs (27.4 ± 6.3 nm, 48.6 ± 5.3 nm, and 104.4 ± 10.3 nm). Ag NPs were washed with deionized water 3 times, prior to supporting on SiO_2.

1.3 Synthesis of SiO_2 nanoparticles. SiO_2 NPs with a diameter of 50 nm were synthesized via a modified Stöber method.[2] Typically, 50 mL of an ethanol solution containing 0.72 mL of H_2O and 2.53 mL of $NH_3 \cdot H_2O$ was stirred at 1200 rpm at 35 °C for 30 min. Then 1.675 mL of TEOS was quickly added and the mixture was stirred for 20 hours. The resultant SiO_2 nanospheres were washed with deionized water 3 times and then dried under vacuum.

1.4 *Ag(2.5 wt%)/SiO_2 catalyst synthesis*: The desired amount of as synthesized Ag NPs were dissolved in 10 mL of deionized water and added to an SiO_2 NP solution contained in a round

bottom flask. The solution was mixed thoroughly at 70 °C for 1 hour and dried at 80 °C using rotary evaporator.

1.5 Characterization. Transmission electron microscope (TEM) images were taken with a FEI-Tecnai 12 TEM facility operating at an accelerating voltage of 200 keV. Specimens prepared from suspension in distilled water were deposited on copper grids coated with a lacey carbon. Average metal particle sizes were measured based on the diameter of 100 particles from corresponding TEM images of each catalyst.

Ultraviolet-visible (UV-Vis) extinction measurements were performed on a Thermo Scientific Evolution 300 spectrophotometer. For both solution phase and diffusion reflectance samples, extinction spectra were collected in the wavelength range of 300 to 700 nm, and all spectra were normalized. Approximately 0.5 mL of the as-synthesized silver nanoparticles, which has a Ag concentration of ~3 mg/mL (depending on the Ag nanoparticle size), were taken into cuvettes vails and diluted further to a final volume of approximately 5 mL with deionized (DI) water. DI water served as the reference spectrum. For diffuse reflectance spectra, solid catalysts were diluted with commercial SiO_2 at roughly a 10:1 ratio. These solid samples were then mounted inside a Harrick Praying Mantis mounted inside of a ThermoScientific Praying Mantis diffuse reflectance adapter. A mirror served as the reference spectrum.

2. Photocatalytic reactivity measurements

All catalytic experiments were performed in a Harrick High Temperature Reaction Chamber and operated under differential reactor conditions (i.e. reactant conversion < 5%). 20.0 mg of catalyst was loaded on top of inert ~7.5 mg SiO_2 gel (60-200 mesh, pore size 150 Å, Sigma Aldrich) to raise the bed height. For pre-treatment and catalytic measurements, ultra-high purity gases, N_2

(99.999%), O_2 (99.999%), and C_2H_4 (99.9%), were purchased from Airgas and used as received. All catalysts were pretreated in situ at atmospheric pressure by flowing 20 sccm (standard cubic centimeters per minute) N_2 and 5 sccm O_2 at 300°C for 3 hours, this removed any remaining ligands from synthesis.

After pretreatment, catalysts were treated at 250 °C with N_2 (15 sccm), C_2H_4 (5 sccm) and O_2 (5 sccm), with total flow rate of 25 sccm, and left overnight (typically, ~12 hours) to reach steady state. Thermal rates were maintained at identical rates (3.5×10^{15} molecule/sec) for all catalysts prior to photocatalytic measurements, by slightly adjusting the reactor temperature. Temperatures of 204 °C, 201 °C, 195 °C and 198 °C were used for the 14.1 nm, 27.4 nm, 48.6 nm, and 104.4 nm Ag particles supported on SiO_2 catalysts, respectively. The constant background thermal rates are necessary to ensure even footed comparison of the photocatalytic properties. The surface temperature in the catalyst bed was measured by thermocouple and optical pyrometer.[3,4] We also measured the temperature of the top of the catalyst bed (where light is primarily absorbed) as a function of illumination intensity (Figure S6). The temperature variation was only ~1.5K up to a photon flux of ~750 mW/cm^2 from a 425 nm LED excitation source. This small variation in catalyst surface temperature provides evidence that equilibrium heating was not responsible for the majority of the observed photoctalytic reactivity.

Photocatalytic measurements were performed by irradiating the catalyst with laser light (NKT Photonics, SuperK FIANIUM, High Power Supercontinuum Laser) in the intensity range 550 to 800 mW/cm^2. Photon wavelength and flux were controlled using the CONTROL software before each measurement, and Fluxes and wavelengths were confirmed via CCD and thermopile detectors**.** LED sources (100W LED CHIP, UV, V(F): 30-34V I(F): 3000mA, CHANZON) were used for lower wavelength studies of 425, 405, and 385 nm. The intensity from the LED was

controlled using a power supply, to match that of the laser flux and was monitored via CCD and thermopile detectors. Photon flux and wavelength dependent measurements were performed at steady state catalytic conditions. The temperature in the catalytic bed was actively controlled via PID controllers. No significant temperature excursions were measured during illumination, and even if slight temperature increases occurred, the online PID would correct for this by decreasing the current to the reactor heaters.

Photocatalytic rates and wavelength dependent measurements of quantum yields (QY) were calculated using the equations below. Constant thermal reaction rates (3.5×10^{15} molecules/s) were used in all measurements. The reported QY in the main text are the internal QY (equation 3 below), and were an average of 2 distinct measurements. The distinct measurements involved reloading the reactor with a new batch of catalyst and following the protocol described above. The small QY error bars show the reproducibility of the measurements.

Equation.1: Photocatalytic rate (molecules/s) = Photothermal rate (molecules/s) – Thermal rate (molecules/s)

Equation.2: QYs (molecules/Photon) = Photocatalytic rate (molecule/s)/Photon flux(photo/s)

Equation.3: Internal QYs = QYs/(1-scattered photon ratio)

3. Electromagnetic simulations

The optical properties of Ag nanoparticles were simulated using the Finite-Difference Time-Domain (FDTD) method for solving Maxwell's equations. This study employed the package from Lumerical FDTD Solutions (Version 8.19). Ag was modeled as spheres of the appropriate diameter and the dielectric function "Ag (Silver) – CRC" was used from the material database provided by Lumerical. A uniform mesh was used with a mesh step of dx = dy = dz = 0.5 nm.

Total-field/scattered-field light source conditions were used in all simulations. The absorption and scattering were calculated within the total-field/scattered-field formalism. For comparison of electromagnetic field enhancement with experimentally determined QY data, the spectral width was determined by the weighted average (weighted using the measured standard deviation) of three simulated extinction spectra of Ag spheres with varying size around the mean particle size (Figure S7). Particle sizes were based on the size distribution determined by TEM (Figure 1C-F). This did not accurately predict to the peak position, however, as there is a well-known but not well-defined oxide layer on Ag that is difficult to model accurately. Specifically, there has been a long-standing debate regarding the nature of the Ag surface under ethylene epoxidation conditions from the surface science and catalysis communities. It is agreed that there is surface oxygen under reaction conditions, but there is no agreement as to the structure of the surface oxide, the coverage of the oxide (i.e. there may be some areas of bare Ag), the location of the oxide (at steps and edges or flat surfaces) or the existence of sub-surface oxygen. This makes modeling of the oxide layer intangible.

To account for the difficulty in modeling the oxide layer on Ag, the size-averaged spectrum was adjusted to be half way between the simulated peak maximum in vacuum and the experimental post reaction UV-vis (Figure S1), in which a more complete Ag oxide layer would be expected. Specifically, the peak maximum for the 12 nm spectrum was shifted by 40 nm, the 25 nm spectrum by 39 nm, the 50 nm spectrum by 41 nm, and the 100 nm spectrum by 25 nm, relative to the vacuum simulation. We note that this shift makes no impact on the conclusions drawn here, as we do not quantitatively compare the position of the peak in QY and peak in modeled light extinction. Instead we highlight wavelength and size dependent ***trends***, which are sufficiently unique to enable differentiation of the near field and hot electron mechanism.

Because the relative hot carrier density and relative surface electric field enhancement varied in distinct ways (surface field strength varied by 2.5-fold as a function of particle size, while hot carrier density varied by > 3 orders of magnitude), these effects could be differentiated by comparison to experiment without perfect matching of the wavelength dependence.

The x-axis adjustment was applied to the electromagnetic field enhancement curves used for qualitative comparison to experiment, as in Figure 3 and S8. The electromagnetic field enhancement of the Ag nanoparticle surface at the surface and within 10 nm of the particle surface (Figure S8) was determined using monitors in the plane parallel to the oscillating electric field of the incident light at a resolution of the mesh (0.5 nm pixels). The intensity of the field enhancement was determined by the following equation[5]:

Equation 4: Electric Field Enhancement = $\frac{1}{A}\int |E(r)|^2/|E_0|^2 \, dr$

For which *r* represents the distance from the surface, which is 0.5 nm in our case. *E(r)* represents the electric field over this area, and *A* represents the area over which the field was integrated (the circumference of the sphere + 1 nm multiplied by the pixel width in the simulation). We performed the integral on the z-plane where the highest field enhancements were observed (in parallel with the incoming field polarity). We performed similar integrals at different azimuthal and polar angles and found no significant difference in the trend of the electric field between particle sizes. Because the incoming field was defined as 1 ($|E_0|^2/|E_0|^2$), the integration provides an electric field enhancement.

To analyze the plasmon induced hot carrier density in the Ag spheres, we followed the approach of Nordlander et al.[5,6] Using a comparison of Schottky barrier devices and theoretical calculations it was demonstrated that hot carrier density in plasmonic nanostructures can be

accurately modeled by integrating the electric field within a mean free path of the nanostructured surface.[5,6]

Thus, for analysis of the hot charge carrier density, the following equation was used:

Equation 5: Hot Charge Carrier Density = $\frac{1}{V_{MFP}}\int_{surf}^{r_{MFP}}|E(r)|^2/|E_0|^2\,dr$

Where V_{MFP} is the volume of the integrated field enhancement from the surface (*surf*) to within to the mean free path of an electron in Ag (r_{MFP}). In this case, V_{MFP} is the volume of the entire spherical particle as the mean free path of electrons in Ag is about the same as the radius of the largest considered particles.. We note that similar to our approach with the surface field enhancement calculation, the integration here was done only on a single z-slice through the sphere. We performed the integral on the z-plane where the highest internal field enhancements were observed (in parallel with the incoming field polarity). We performed similar integrals at different azimuthal and polar angles and found no significant difference in the trend as a function of particle size.

4. Monte-Carlo simulations

The optical properties of Ag spheres of different size and one silica sphere in air were both performed by the finite-difference-time-domain (FDTD) method (Lumerical solutions 2018a). CRC and Palik database were used for the Ag and silica refractive indices, respectively. The absorption and scattering cross-section of a single Ag or silica sphere in air was calculated using the broad-band multi-frequency total-field-scattered-field (TFSF) approach with normal incident light. The absorption cross sections were calculated from the total field power flux through a closed surface. The scattering cross sections were calculated from the scattered field power flux through a closed surface.

The Monte-Carlo approach was used to determine the photon escape ratio (the fraction of impinging photons that scattered out of the reactor bed) from the 2.5 mm layer of randomly distributed Ag spheres in silica matrix on top of 1 mm layer of silica gel in a cylindrical chamber (a model of the experimental system). Perfect reflection was assumed for photon reflection from the cylindrical chamber wall and bottom surface. The Monte-Carlo simulation code was custom written in C language. To model normal incident uniform light illumination on the catalyst bed, the position of injected photons were placed at the bed surface with velocity normal to the surface. The photon transport distance, x, between photon-particle interaction events was assumed to follow a random distribution with the probability density function of $\alpha \cdot e^{\alpha \cdot x}$, where α is the extinction coefficient, which is a sum of the scattering coefficient, α_s, and absorption coefficient α_a. The scattering coefficient α_s is equal to the Ag sphere scattering cross section times Ag particle density, plus the silica sphere scattering cross section times silica sphere particle density. Since lossless silica is used, the absorption coefficient α_a is equal to the Ag sphere absorption cross section times Ag particle density. When a collision event occurs (ie a photon impinges on an Ag particle), $\alpha_a/(\alpha_a + \alpha_s)$ portion of photon energy is absorbed and the photon is scattered into new direction following the unpolarized dipole far-field scattering profile. The transport of a single photon continues until the photon energy is lower than a threshold level (considered totally absorbed) or escaped from the catalyst bed.

5. Supplemental Figures

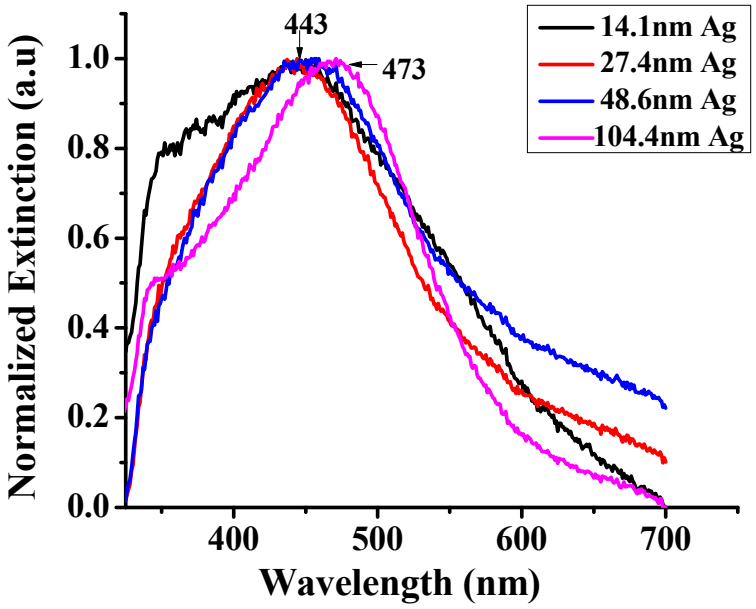

Figure S1. Diffuse reflectance UV-vis spectra of the used catalysts. These spectra were collected after 60 hours on stream under reaction conditions.

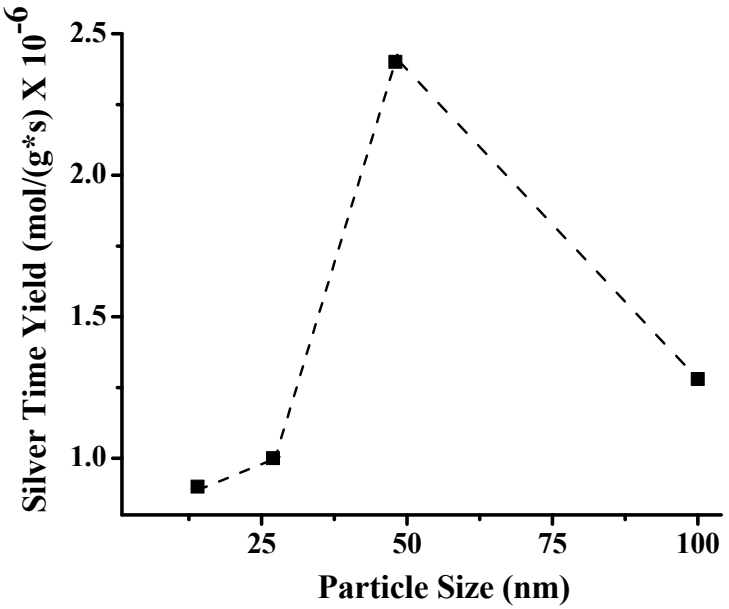

Figure S2: The influence of Ag nanoparticle size on thermal reactivity for the ethylene oxidation reaction. These experiments were performed with 10 wt% Ag on SiO_2 catalysts (all photocatalytic measurements were made is 2.5 wt% Ag to minimize hot spot formation) and 25sccm total gas flow of 15sccm N_2: 5sccm O_2: 5sccm C_2H_4 were used for this reaction. 48.6nm Ag catalyst showed the highest silver time yield (these units were used to compare to reference 5), which decreased in the order of 48.6 nm > 104.4 nm > 27.4 nm > 14.1 nm. These results are well correlated with previous published literature, demonstrating that the colloidal synthesis is consistent with impregnation based synthesis approaches.[7]

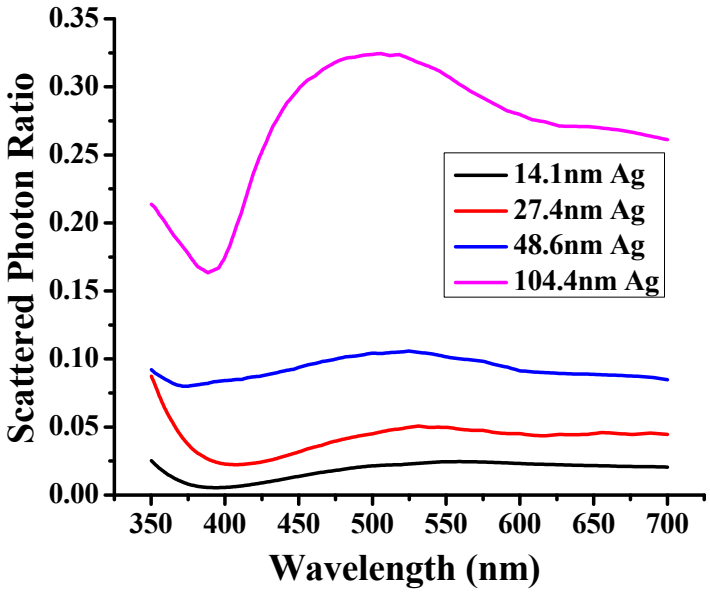

Figure S3: Wavelength-dependent fraction of photon scattered out of the catalyst bed for Ag@SiO_2 with different Ag NP sizes derived from Monte Carlo simulations.

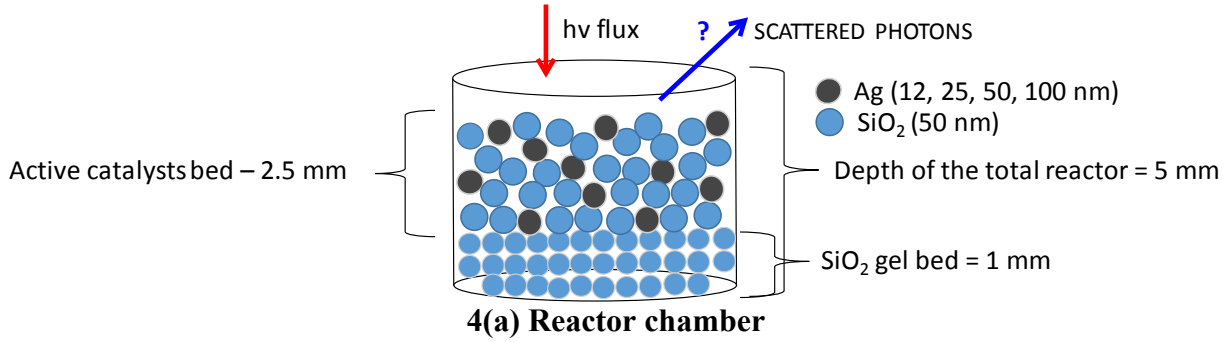

4(a) Reactor chamber

4(b) Ag and SiO_2 Particle concentration in reactor

Catalyst (Ag/SiO_2), SiO_2 – 50 nm	**Density N/V (particles/ cm^{-3})**	
	Ag	**SiO_2**
Ag (100 nm)/SiO_2	2.06E+12	7.15E+14
Ag (50nm)/SiO_2	1.65E+13	7.15E+14
Ag (25 nm)/SiO_2	1.32E+14	7.15E+14
Ag (12 nm)/SiO_2	1.19E+15	7.15E+14

4(c) Fraction of escaped photons

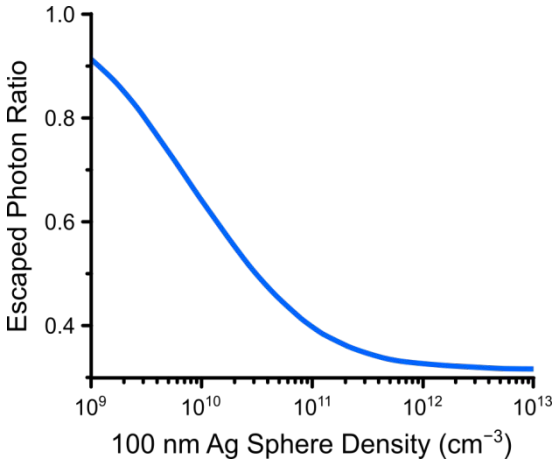

Figure S4: (a) Determination of escaped photon ratio from the 2.5 mm layer of randomly distributed Ag spheres in silica matrix on top of 1 mm layer of silica gel in a cylindrical chamber by Monte-Carlo approach. (b) Density of Ag and SiO_2 particles in the reactor bed. (c) The fraction of escaped photons calculated by Monte-Carlo simulations for 100 nm Ag particles as a function of particle density in the reactor at 500 nm wavelength of light.

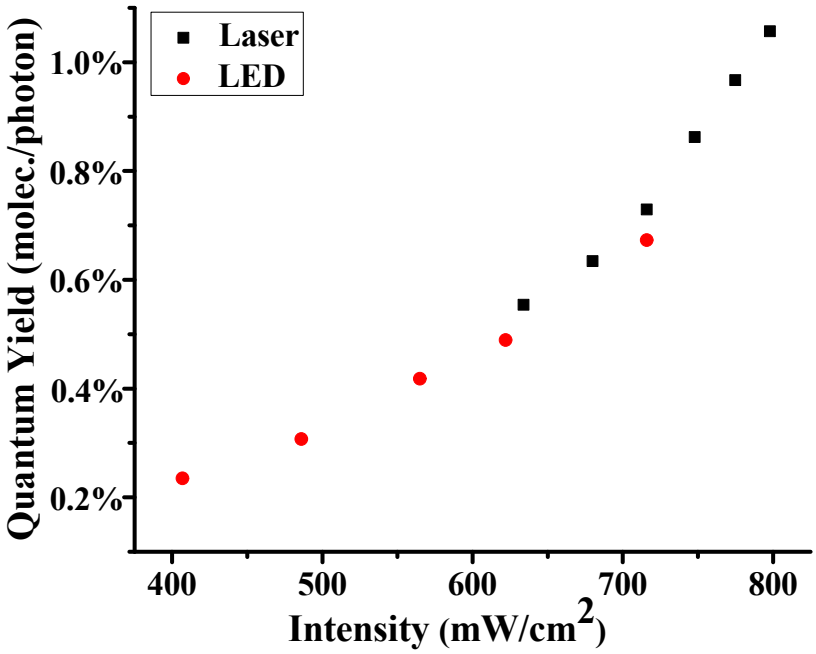

Figure S5: Comparison of ethylene oxidation quantum yields as a function of wavelengths for Laser and LED illumination on 104 nm Ag particles. Because the laser wavelengths are limited to 425 nm, lower wavelength of 425 nm, 405 nm and 385 nm were studied with LEDs. At 425 nm both LED and Laser quantum yields were close and comparable at the same flux of 716 mW/cm^2.

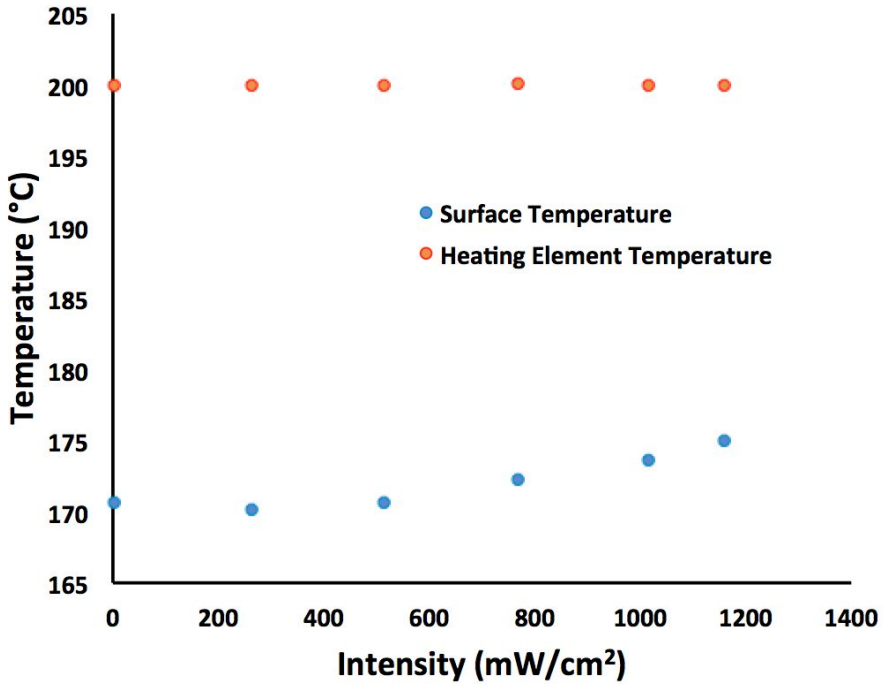

Figure S6: Measurement of the temperature at the top of the catalyst bed (surface temperature) and heating element for 14 nm Ag particle catalyst as a function of photon flux from a 425 nm LED source. The existing temperature gradient in the bed is due to the heating element location underneath the catalyst bed. The heating element temperature measurement was used along with a PID controller to maintain a constant temperature in the system. The surface temperature is the one reported throughout the paper. It is critical to notice that the surface temperature varied only slightly (by 1.5 K) at the photon flux (750 mW/cm^2) used in a majority of our study. This provides direct evidence that equilibrium thermal heating was not responsible significantly for the observed photocatalytic reactivity.

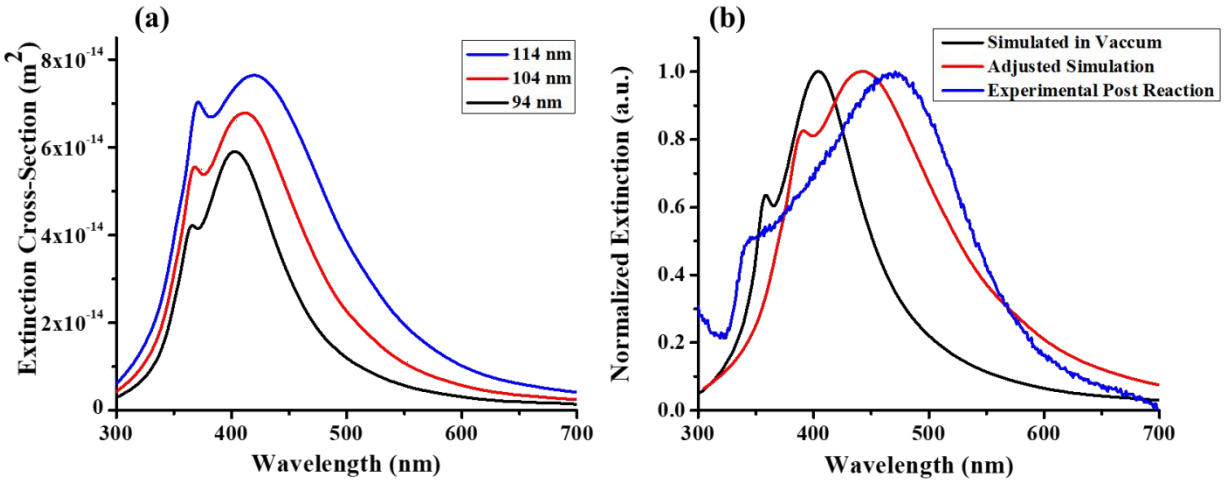

Figure S7. Method of adjustment for FDTD simulations to compare with experiment, shown here for 104.4 nm Ag particles. (A) FDTD simulations of extinction spectra of three Ag spheres on SiO_2, which were weighted and averaged to adjust for heterogeneous spectral broadening. Particle sizes were based on the size distribution determined by TEM. (B) FDTD simulation of a single 104.4 nm sphere in vacuum (black), the experimental post-reaction UV-vis (blue), and the simulated size distribution averaged spectrum (red) positioned half way between the vacuum and experimental post-reaction UV-vis, which was done to approximate the refractive index environment during reaction.

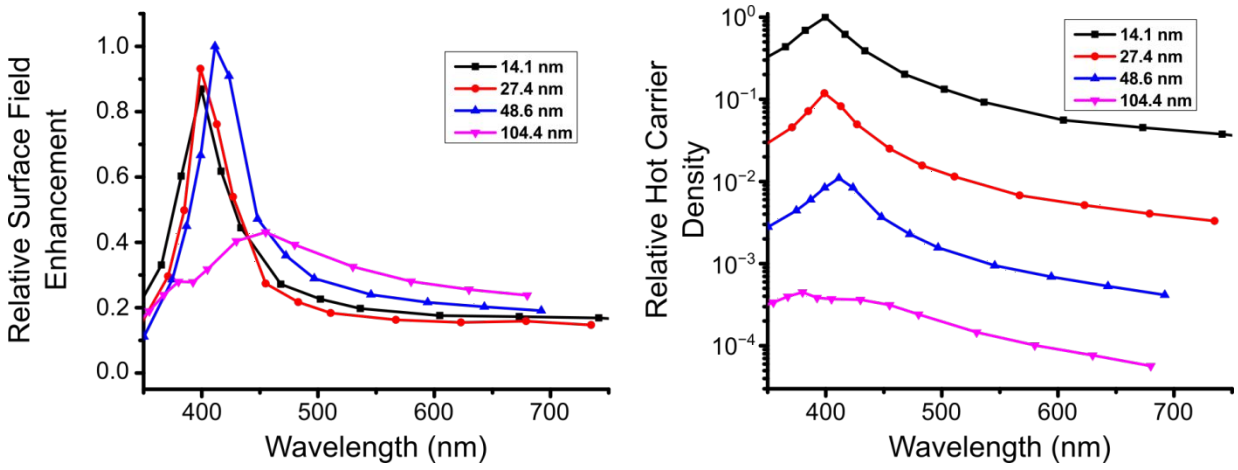

Figure S8. (A) The relative electromagnetic field enhancement at the surface and (B) the relative hot charge carrier density for all four considered particle sizes.

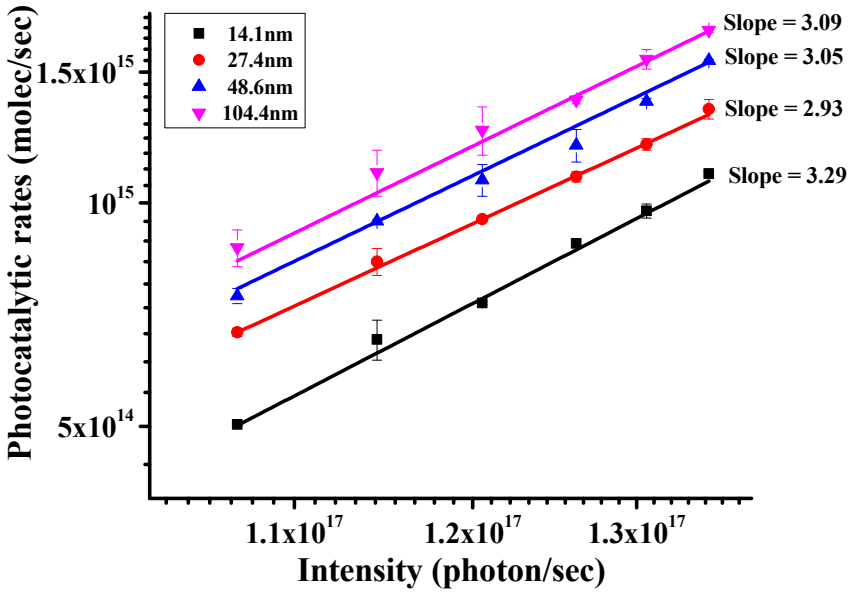

Figure S9: Influence of light flux on photocatalytic rates using 500 nm photons for the Ag(2.5 wt%)/SiO_2 catalysts. A 25 sccm total gas flow of 15sccm N_2: 5sccm O_2: 5sccm C_2H_4 was used for these reactions. Prior to these reactions, thermal catalytic rates were maintained to be the same (3.5 x 10^{15} molecule/sec).

References

(1) Bastús, N. G.; Merkoçi, F.; Piella, J.; Puntes, V. Synthesis of Highly Monodisperse Citrate-Stabilized Silver Nanoparticles of up to 200 Nm: Kinetic Control and Catalytic Properties. *Chem. Mater.* **2014**, *26*, 2836–2846.

(2) Stober, W.; Fink, A.; Bohn, E. Controlled Growth of Monodisperse Silic Spheres in the Micron Size Range. *J. Colloid Interface Sci.* **1968**, *26*, 62–69.

(3) Kale, M. J.; Christopher, P. Utilizing Quantitative in Situ FTIR Spectroscopy to Identify Well-Coordinated Pt Atoms as the Active Site for CO Oxidation on Al2O3-Supported Pt Catalysts. *ACS Catal.* **2016**, *6*, 5599–5609.

(4) Li, X.; Zhang, X.; Everitt, H. O.; Liu, J. Light-Induced Thermal Gradients in Ruthenium Catalysts Significantly Enhance Ammonia Production. *Nano Lett.* **2019**, *19*, 1706–1711.

(5) Zheng, B. Y.; Zhao, H.; Manjavacas, A.; McClain, M.; Nordlander, P.; Halas, N. J. Distinguishing Between Plasmon-Induced and Photoexcited Carriers in a Device Geometry. *Nat. Commun.* **2015**, *6*, 7797.

(6) Manjavacas, A.; Liu, J. G.; Kulkarni, V.; Nordlander, P. Plasmon-Induced Hot Carriers in Metallic Nanoparticles. *ACS Nano* **2014**, *8*, 7630–7638.

(7) van den Reijen, J. E.; Kanungo, S.; Welling, T. A. J.; Versluijs-Helder, M.; Nijhuis, T. A.; de Jong, K. P.; de Jongh, P. E. Preparation and Particle Size Effects of Ag/A-Al2O3 Catalysts for Ethylene Epoxidation. *J. Catal.* **2017**, *356*, 65–74.